Estimates on the convergence of expansions at finite baryon chemical potentials

Rui Wen,[1,*] Shi Yin,[2] and Wei-jie Fu[3]

[1]*School of Nuclear Science and Technology, University of Chinese Academy of Sciences, Beijing, 100049, Peoples Republic of China*

[2]*Institut für Theoretische Physik, Justus-Liebig-Universität Gießen, 35392 Gießen, Germany*

[3]*School of Physics, Dalian University of Technology, Dalian, 116024, Peoples Republic of China*

(Received 19 March 2024; accepted 14 June 2024; published 9 July 2024)

Convergence of three different expansion schemes at finite baryon chemical potentials, including the conventional Taylor expansion, the Padé approximants, and the T' expansion proposed recently in lattice QCD simulations, have been investigated in a low energy effective theory within the functional renormalization group approach. It is found that the convergence of the T' expansion and the Padé approximants is consistent with the conventional Taylor expansion, within the expansion orders considered in this work. Furthermore, we find that the consistent regions of the three different expansions are in agreement with the convergence radius of the Lee-Yang edge singularities.

DOI: 10.1103/PhysRevD.110.016008

I. INTRODUCTION

Knowledge of the QCD phase structure, and in particular locating the critical end point (CEP), has been widely discussed during the past few decades. Both experimental and theoretical studies have made significant progress. On the experimental side, the Beam Energy Scan (BES) program at the Relativistic Heavy Ion Collider (RHIC) have measured the high order cumulants of net-proton distributions [1–5], which are thought of as ideal probe to detect the CEP. On the theoretical side, lattice QCD simulations are employed to calculate the equation of state [6–8] and baryon number fluctuations [9–13] at vanishing chemical potentials. However, lattice simulations are limited to imaginary and vanishing chemical potential due to the sign problem. On the other hand, the first principles functional approaches, such as the functional renormalization group (fRG) [14–18] and Dyson-Schwinger equation (DSE) [19–22], do not suffer from the sign problem and allow us to do direct calculations at real chemical potentials. Recently, the functional approaches have shown convergent estimates for the location of CEP in the phase diagram, which is in a small region of $\mu_B \in (600, 650)$ MeV with $\mu_B/T > 4$ [14,19,21]. In the region of large baryon chemical potentials, errors of calculation resulting from truncations in the functional methods might increase sizably, which have to be controlled carefully via, e.g., comparison with lattice QCD and functional QCD of improved truncations. For recent reviews, see, e.g., [23–27].

In the past few years, lots of efforts have been made to extend lattice QCD results into finite chemical potentials. In [9,28], the Taylor expansion method is employed to extend the equation of state and the baryon number fluctuations into nonzero chemical potential. Due to the negative values of both χ_6^B and higher order susceptibilities [10–12], the pressure and baryon-number density with the Taylor expansion method show nonmonotonic behavior at $\mu_B/T \gtrsim 2.5$ [28], which implies the Taylor expansion method becomes less reliable in this region. Note that the reliability of Taylor expansion can be improved by including increasingly higher orders, while the radius of convergence of the series can not. One can use the reliability region of increasingly higher orders to estimate the convergence radius of expansion. It is generally believed that the convergence radius of the Taylor expansion is limited by singularities in the complex plane of chemical potentials, such as the Lee-Yang edge singularities [29–34] and the Roberge-Weiss transition singularities [35]. Besides, the Padé resummation [36–39] and other resummation method [33,40] are also investigated widely, and a sign reweighting method, which allows for direct simulations at real baryon densities, is also proposed in [41–43].

In [44], the Wuppertal-Budapest Collaboration has proposed a T' expansion scheme, which extrapolates the pressure and baryon number density at imaginary and vanishing chemical potentials to those at real ones. The rescaling coefficients are related with Taylor expansion

*Contact author: rwen@ucas.ac.cn

coefficients. So in other words, they also provide a resummation scheme of the Taylor expansion coefficients. Since the statistical errors of χ_1^B, χ_2^B at imaginary chemical potentials are quite small in lattice QCD simulations, the statistical errors of the extrapolation are well controlled. Recently, the expansion scheme was generalized with the strangeness neutrality condition [45].

Nonetheless, the convergence radius of the T' expansion scheme is still unclear. In this work, we investigate the convergence radius of the new expansion scheme and compare it with the Taylor expansion and the Padé resummation. The Polyakov-loop extended quark-meson (PQM) model is employed, which can well describe the chiral symmetry breaking/restoration and confinement/deconfinement phase transitions. Baryon number fluctuations obtained in this effective theory are in good agreement with lattice QCD results [46–48].

This paper is organized as follows: In Sec. II, the Polyakov-loop extended quark-meson model within the fRG approach at real and imaginary chemical potential is introduced. In Sec. III, we briefly review the expansion scheme and give the formulas of higher-order generalized susceptibilities. In Sec. IV, we give the numerical results. The summary and conclusion are given in Sec. V.

II. TWO-FLAVOR POLYAKOV-LOOP EXTENDED QUARK-MESON MODEL

We employ the two-flavor Polyakov-loop extended quark-meson model within the functional renormalization group approach [46–52], which is a QCD low energy effective theory. The Euclidean effective action reads

$$\Gamma_k = \int_x \Big\{ Z_{q,k}\bar{q}[\gamma_\mu\partial_\mu - \gamma_0(\mu + igA_0)]q + \frac{1}{2}Z_{\phi,k}(\partial_\mu\phi)^2 + h_k\bar{q}(T^0\sigma + i\gamma_5\vec{T}\cdot\vec{\pi})q + V_k(\rho) - c\sigma + V_{\text{glue}}(L,\bar{L})\Big\}, \tag{1}$$

with a four-dimensional integral $\int_x = \int_0^{1/T} dx_0 \int d^3x$. Here, T, μ are the temperature and the quark chemical potential, respectively. The baryon chemical potential reads $\mu_B = 3\mu$. The meson field reads $\phi = (\sigma, \vec{\pi})$ and $V_k(\rho)$ denotes a chiral symmetric effective potential with $\rho = \phi^2/2$. The chiral symmetry is explicitly broken by the linear sigma term $-c\sigma$. A_0 denotes the gluon background field. $L(A_0)$ is the traced Polyakov loop, and $\bar{L}(A_0)$ is its conjugate, which are defined as

$$L(x) = \frac{1}{N_c}\langle \mathrm{Tr}\mathcal{P}(x)\rangle, \qquad \bar{L}(x) = \frac{1}{N_c}\langle \mathrm{Tr}\mathcal{P}^\dagger(x)\rangle, \tag{2}$$

with

$$\mathcal{P}(x) = \mathcal{P}\exp\left(ig\int_0^\beta d\tau A_0(x,\tau)\right), \tag{3}$$

and $\mathcal{P}$ is the path ordering operator. The V_{glue} denotes the glue potential, which is a function of the traced Polyakov loop L and $\bar{L}$.

In this work, we adopt the local potential approximation (LPA), where the dependence of the wave function renormalizations and Yukawa coupling on the renormalization group (RG) scale is neglected, i.e., $Z_{q/\phi,k} = 1$, $\partial_k h_k = 0$. We choose the ultraviolet cutoff scale $k_{\text{UV}} = 700$ MeV, the initial potential $V_{\text{UV}}(\rho) = \lambda_1\rho + \lambda_2\rho^2/2$ with $\lambda_1 = 482^2$ MeV^2, $\lambda_2 = 5.7$. Moreover, one has the Yukawa coupling $h = 6.5$ and the explicitly chiral symmetry breaking coefficient $c = 1.7\times10^6$ MeV^3, fixed by fitting the physical observables in the vacuum: $f_\pi = 92$ MeV, $m_q = 300$ MeV, $m_\pi = 135$ MeV and $m_\sigma = 500$ MeV. The parametrization of the Polyakov loop potential is used as same as that in [47].

We proceed with the flow equation of $V_k(\rho)$, which reads

$$\partial_k V_k(\rho) = \frac{k^3}{4\pi^2}[3l_0^{(B)}(m_\pi) + l_0^{(B)}(m_\sigma) - 4N_cN_f l_0^{(F)}(m_f)]. \tag{4}$$

Here, $N_c = 3$, $N_f = 2$, and $l_0^{(B/F)}$ are bosonic/fermionic loop functions, which can be found in [46,47,53]. Note that when the chemical potential is purely imaginary, the fermionic distribution functions are complex valued. The antifermionic distribution function is the complex conjugate of the fermionic one, and thus, we are left with a real fermionic loop function,

$$\begin{aligned} l_0^{(F)}(m_f) &= \frac{k}{3E}(1 - n_f(L,\bar{L}) - \bar{n}_f(\bar{L},L)) \\ &= \frac{k}{3E}[1 - 2\mathrm{Re}(n_f)], \end{aligned} \tag{5}$$

which ensures that the effective potential and physical observables are real valued. Whereas, if the chemical potential is a general complex number, the imaginary part of the fermionic loop function would be nonzero.

The chiral pseudocritical temperature of PQM model, which is determined by the location of peak of $|\partial m_f/\partial T|$, is $T_c = 215$ MeV at $\mu_B = 0$. Following [47], we use the scale matching between the $N_f = 2$ PQM model and the $N_f = 2+1$ QCD,

$$T_{\text{QCD}}^{(N_f=2+1)} = cT_{\text{PQM}}^{(N_f=2)} \tag{6}$$

$$\mu_{B\text{QCD}}^{(N_f=2+1)} = c\mu_{B\text{PQM}}^{(N_f=2)}, \tag{7}$$

with

$$c = \frac{T_{c\mathrm{QCD}}^{(N_f=2+1)}}{T_{c\mathrm{PQM}}^{(N_f=2)}} = \frac{156\ \mathrm{MeV}}{215\ \mathrm{MeV}} = 0.726. \tag{8}$$

The continuous crossover becomes increasingly sharper with the increase of the baryon chemical potential, and $|\partial m_f/\partial T|$ finally diverges at the CEP, that allows us to locate the CEP with $T_{\mathrm{CEP}} = 40$ MeV, $\mu_{B_{\mathrm{CEP}}} = 667$ MeV after the rescaling. Note that the temperature of the CEP T_{CEP}, obtained here in the PQM model with the LPA truncation, is smaller than that obtained in the first principles functional QCD [14,19,54]. This is also observed in other calculations in low energy effective models, e.g., [33,52,55]. This defect has been circumvented in QCD-assisted low energy effective theories; see [47,48] for more relevant discussions. The CEP in QCD is a second-order phase transition point and belongs to the Ising-like $Z(2)$ universality class [56]. Various susceptibilities are divergent at the CEP. The CEP can also be connected to the Lee-Yang edge singularity at the real axis of the complex plane of baryon chemical potential [33].

III. EXPANSION SCHEME

The generalized susceptibilities of the baryon number are defined as ith order derivatives of the normalized pressure,

$$\chi_i^B = \frac{\partial^i}{\partial \hat{\mu}_B{}^i}\frac{p}{T^4}, \tag{9}$$

with $\hat{\mu}_B = \mu_B/T$. We numerically calculate the generalized susceptibilities up to 10th order in this work, and an algorithmic differentiation technique for higher-order derivatives calculation is proposed in [36,57].

The Taylor expansion of the pressure is given as

$$\frac{p(T,\hat{\mu}_B) - p(T,0)}{T^4} = \sum_{n=1}\frac{1}{(2n)!}\chi_{2n}^B(T,0)\hat{\mu}_B^{2n}. \tag{10}$$

In the following, we will introduce another two expansion schemes, i.e., the Padé approximants and T' expansion.

A. Padé approximants

We introduce the Padé approximants to reconstruct the pressure as a function of $\hat{\mu}_B^2$,

$$P[m,n] \equiv \frac{p(T,\hat{\mu}_B) - p(T,0)}{T^4} = \frac{\sum_{i=1}^{n/2} a_i \cdot \hat{\mu}_B^{2i}}{1 + \sum_{j=1}^{m/2} b_j \cdot \hat{\mu}_B^{2j}}. \tag{11}$$

Here, the coefficients a_i, b_i are determined by solving the equations,

$$\frac{\partial^i P[m,n]}{\partial \hat{\mu}_B{}^i} = \chi_i^B. \tag{12}$$

In this work, we mainly consider $P[4,2]$, $P[4,4]$ and $P[6,4]$, which correspond to reconstructing the first 6th, 8th, and 10th order susceptibilities, respectively. Explicit expressions of $P[m,n]$ are given in the Appendix. The generalized susceptibilities are ith order derivatives of the Padé approximants of the pressure with respect to $\hat{\mu}_B$. One can also calculate the Padé approximants of ith order susceptibilities, but we would not do it, since they are not our main concerns in this work. Moreover, the poles of the Padé approximants can be used to estimate the convergence radius of Taylor expansion, e.g., the poles of $P[n,2]$ and $P[n,4]$ are related to the ratio estimator and Mercer-Roberts estimator [35,39], respectively, which are given by

$$r_{c,2n}^{\mathrm{ratio}} = \left|\frac{(n+1)(n+2)\chi_{2n}^B}{\chi_{2n+2}^B}\right|^{\frac{1}{2}}, \tag{13}$$

$$r_{c,2n}^{\mathrm{MR}} = \left|\left[\frac{\chi_{2n+2}^B\chi_{2n-2}^B}{(2n+2)!(2n-2)!} - \left(\frac{\chi_{2n}^B}{(2n)!}\right)^2\right]\right|^{\frac{1}{4}} \times \left|\left[\frac{\chi_{2n}^B\chi_{2n+4}^B}{(2n)!(2n+4)!} - \left(\frac{\chi_{2n+2}^B}{(2n+2)!}\right)^2\right]\right|^{-\frac{1}{4}}. \tag{14}$$

B. T' expansion scheme

Recently, a relation between the baryon number density $n_B(\hat{\mu}_B)$ at finite chemical potentials and the quadratic baryon number fluctuation $\chi_2^B(\hat{\mu}_B = 0)$ at vanishing chemical potentials has been proposed by the Wuppertal-Budapest Collaboration [44], which reads

$$\frac{\chi_1^B(T,\hat{\mu}_B)}{\hat{\mu}_B} = \chi_2^B(T',0), \tag{15}$$

with

$$T' = T(1 + \kappa_2^B(T)\hat{\mu}_B^2 + \kappa_4^B(T)\hat{\mu}_B^4 + \kappa_6^B(T)\hat{\mu}_B^6 + \kappa_8^B(T)\hat{\mu}_B^8 + \mathcal{O}(\hat{\mu}_B^{10})). \tag{16}$$

Here, $\kappa_{2n}^B(T)$ are expanding coefficients of different orders.

In Fig. 1, we show the $\chi_1^B/\hat{\mu}_B$ as a function of temperature with real and imaginary baryon chemical potentials in the range of $|\hat{\mu}_B| \le 7\pi/8$. Obviously, one arrives at $\chi_1^B/\hat{\mu}_B = \chi_2^B$ at $\hat{\mu}_B = 0$. As we can see, for a fixed value of $\hat{\mu}_B$, either real or imaginary chemical potential, $\chi_1^B/\hat{\mu}_B$ always increase with the temperature monotonically, which is a necessary condition for the rescaling relation in Eq. (15). For a fixed temperature, the ratio $\chi_1^B/\hat{\mu}_B$ also increases with $\hat{\mu}_B^2$ monotonously. The calculated results in Fig. 1 also indicate that the expansion method is only suitable for the temperature around the phase transition [44], i.e., $T \in [80, 220]$ MeV

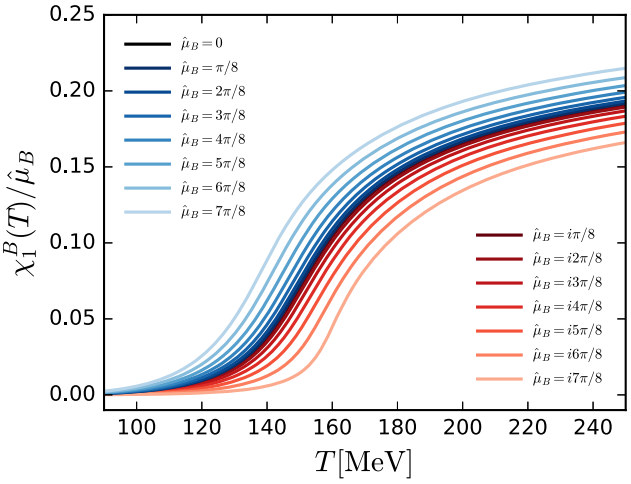

FIG. 1. Ratio $\chi_1^B/\hat{\mu}_B$ as a function of the temperature with real (blue) and imaginary (red) baryon chemical potentials, which coincides with the quadratic fluctuation χ_2^B exactly at $\hat{\mu}_B = 0$.

for this work, because the ratio $\chi_1^B/\hat{\mu}_B$ becomes flat at low or high temperatures. Furthermore, at large $|\hat{\mu}_B|$, the shape of $\chi_1^B/\hat{\mu}_B$ becomes different from that of $\chi_2^B(\mu_B = 0)$, which implies that the rescaled temperature and expansion scheme may no longer work in that region.

The coefficients κ_{2n}^B can be calculated by fitting the results at zero and imaginary chemical potentials. In Fig. 2, we show the rescaled temperature $T'(T, \hat{\mu}_B)$, which is defined in Eq. (15), as a function of $\hat{\mu}_B^2$. We choose several original temperatures in the range of $T \in [108, 196]$ MeV. The dots denote the results calculated directly from the fRG approach at both the imaginary and real chemical potentials.

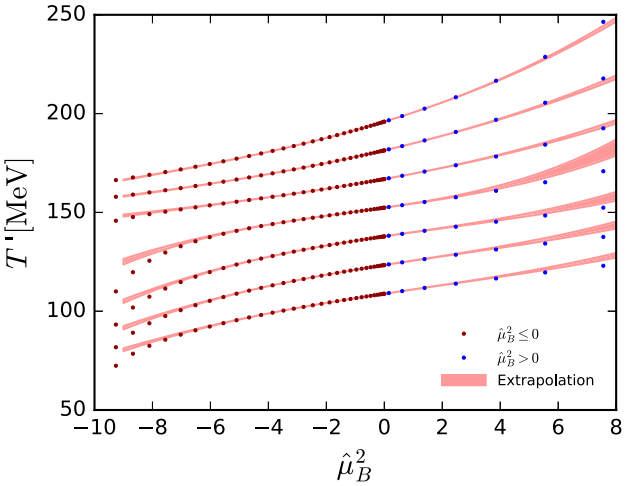

FIG. 2. Rescaled temperature T' defined in Eq. (15) as a function of $\hat{\mu}_B^2$. The original temperature T is chosen in the range of [108, 196] MeV at the interval of 14.5 MeV. The dark-red dots and blue dots stand for results at imaginary and real chemical potentials, respectively. The red bands denote the extrapolation of Eq. (16) from the imaginary to real chemical potentials.

The red bands stand for the polynomial fitting of fRG data at zero and imaginary chemical potentials, cf. Eq. (16), which are also extrapolated into the regime of real baryon chemical potentials. More specifically, the bands are determined by fitting the results of $\mathrm{Im}\hat{\mu}_B \in [0, |\hat{\mu}_B|_{\max}]$. The upper bound $|\hat{\mu}_B|_{\max}$ is varied in the range of [2.0, 2.4] MeV, in order to investigate errors of the fitting, denoted by the width of bands. The comparison between the extrapolation of fitting at imaginary chemical potentials and the direct fRG results at real chemical potentials constitutes a nontrivial test. One can see that the agreement in the region of $|\hat{\mu}_B^2| \lesssim 6$, that is $|\hat{\mu}_B| \lesssim 2.5$, is very well, while there is some difference beyond this regime.

The coefficients κ_{2n}^B can also be calculated from the Taylor expansion coefficients. With the Taylor expansion (10), we arrive at

$$\frac{\chi_1^B(T, \hat{\mu}_B)}{\hat{\mu}_B} = \sum_{n=1} \frac{1}{(2n-1)!} \chi_{2n}^B(T, 0) \cdot \hat{\mu}_B^{2n-2}. \quad (17)$$

Comparing (17) with (15) and (16), one obtains the relations between the two sets of expansion coefficients, which are shown in (A4) through (A11) in the Appendix. Obviously, in the new expansion scheme, the coefficients κ_{2n}^B encode the information of $\chi_2^B \cdots \chi_{2n+2}^B$ as well as $1 \cdots n$th order temperature derivatives of χ_2^B at vanishing chemical potential. For lattice QCD, it is a numerical challenge to precisely calculate the nth order temperature derivatives of χ_2^B. On the other hand, it is feasible for lattice QCD to obtain the coefficients κ_{2n}^B by fitting χ_2^B at several imaginary chemical potentials with Eq. (16) and calculate the temperature derivatives of χ_2^B in turn [44].

In Fig. 3, the coefficients calculated from the fitting of imaginary chemical potentials and the Taylor expansion coefficients in (A8) to (A10) are presented. Obviously, the results obtained from two different methods agree with each other very well. Our results are also comparable with the lattice results [44], in the range of $0.015 \lesssim \kappa_2^B \lesssim 0.03$ with a slight increase in the regime of high temperature, while the high-order coefficients κ_4^B amd κ_6^B are very close to zero. In the following, we use the coefficients calculated from the Taylor expansion coefficients and ignore the errors.

In this expansion scheme, the pressure reads

$$\frac{p(T, \hat{\mu}_B) - p(T, 0)}{T^4} = \int_0^{\hat{\mu}_B} d\hat{\mu}_B' \chi_1^B(T, \mu_B') = \int_0^{\hat{\mu}_B} d\hat{\mu}_B' \hat{\mu}_B' \chi_2^B(T', 0). \quad (18)$$

The first three order generalized susceptibilities are given as

$$\chi_1^B(T, \mu_B) = \hat{\mu}_B \chi_2^B(T', 0), \quad (19)$$

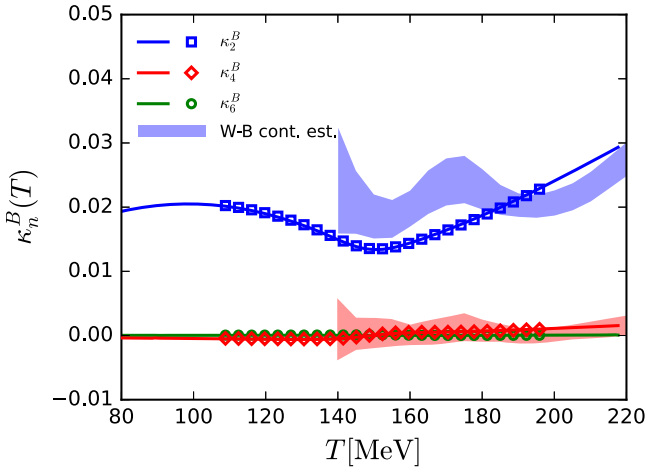

FIG. 3. Coefficients in Eq. (16) as functions of the temperature. The markers denote the results obtained from the fitting of imaginary chemical potentials, and the solid lines stand for those calculated Taylor expansion coefficients in Eqs. (A8) through (A10). The bands indicate lattice results in [44].

$$\chi_2^B(T,\mu_B) = \chi_2^B(T',0) + \hat{\mu}_B \frac{\partial \chi_2^B(T',0)}{\partial T'} \frac{\partial T'}{\partial \hat{\mu}_B}, \tag{20}$$

$$\chi_3^B(T,\mu_B) = 2\frac{\partial \chi_2^B(T',0)}{\partial T'} \frac{\partial T'}{\partial \hat{\mu}_B} + \hat{\mu}_B \left(\frac{\partial^2 \chi_2^B}{\partial T'^2} \left(\frac{\partial T'}{\partial \hat{\mu}_B} \right)^2 + \frac{\partial \chi_2^B}{\partial T'} \frac{\partial^2 T'}{\partial \hat{\mu}_B{}^2} \right). \tag{21}$$

IV. NUMERICAL RESULTS

We plot the pressure and the first three order generalized susceptibilities at several temperatures around the pseudocritical temperature ($T_c = 156$ MeV) in Fig. 4, which are calculated from the Taylor expansion, the Padé approximants, as well as the T' expansion. The full results from fRG are also plotted for comparison. In order to make a meaningful comparison, we only show results using the first eight order generalized susceptibilities, i.e., the Taylor expansion up to 8th order, the Padé approximant $P[4,4]$ and the T' expansion of κ_6^B order. For the pressure, all expansion schemes of different types converge well, and there is only a slight divergence between the full calculated results and the expansion results for $\hat{\mu}_B \gtrsim 3.5$. For the generalized susceptibilities, the consistent region becomes smaller with the increase of μ_B/T, which is $\hat{\mu}_B \lesssim 3.0$, 2.0, 1.5 for $\chi_1^B, \chi_2^B, \chi_3^B$, respectively.

In order to investigate the errors of different expansion schemes in detail, we show the relative difference of χ_2^B between the expansion results and full results in the plane of T and $\hat{\mu}_B$ in Fig. 5. Subplots in the first line denote the results obtained with the expansion up to the order of $\mathcal{O}(\chi_6^B)$, and those in the second and third lines to $\mathcal{O}(\chi_8^B)$, $\mathcal{O}(\chi_{10}^B)$, respectively. It is found that with the increase of the expansion order, the convergence is improved mildly. For the Taylor expansion, one can see an alterant structure at large $\hat{\mu}_B$, that is related with the oscillatory structure of the highest order susceptibility. The results of T' expansion of order $\mathcal{O}(\kappa_4)$ are always smaller than the full results, while the structure becomes a bit complicated for the orders $\mathcal{O}(\kappa_6)$ and $\mathcal{O}(\kappa_8)$. Note that the numerical accuracy of T' expansion of $\mathcal{O}(\kappa_8)$ is constrained by numerical precision of $\chi_2^{B(4)}(T)$. The sharp inconsistent lines in the plot of $P[6,4]$ are caused by the poles of the Padé approximant $P[6,4]$ at $T = 146$, 157, 175 MeV.

The convergence radius near the critical temperature, i.e., $T \in (140, 180)$ MeV, is smaller than that in the regimes of high or low temperature. Roughly speaking, the convergence radius is about $\hat{\mu}_B \sim 2$ for χ_2^B in the vicinity of chiral phase transition. A simple explanation is as follows. At low temperature, the system tends towards hadron resonance gas, i.e., $\chi_{2n}^B/\chi_2^B = 1$ for $n \geq 1$, and at high temperature, it tends towards the Stefan-Boltzmann limit, i.e., $\chi_{2n}^B/\chi_2^B = 0$ for $n \geq 3$. Both cases give rise to an infinite convergence radius. Whereas in the proximity of the chiral phase transition, the high order susceptibilities oscillate, and the convergence radius is a finite value.

Strictly speaking, the convergence radius of an expansion can only be defined when it is expanded to infinite orders. In our case, it implies that we have to know the information on the baryon susceptibilities of infinite orders. As we have mentioned above, the convergence radius of the expansion schemes might be constrained by singularities in the complex plane of chemical potential. Here, we consider the Lee-Yang edge singularities, whose convergence radius is given from scaling analysis in [29]

$$R_{\text{conv}} = \left| \frac{z_c}{z_0} \left(\frac{m_l^{\text{phys}}}{m_s^{\text{phys}}} \right)^{\frac{1}{\beta\delta}} - \frac{T - T_c^0}{T_c^0} \right|^{\frac{1}{2}} \frac{1}{\sqrt{\kappa_2}}. \tag{22}$$

Here, $m_l^{\text{phys}}/m_s^{\text{phys}} = 1/27$, and β, δ are critical exponents, and we use fRG results with LPA truncations in [56], i.e., $\beta = 0.3989$, $\delta = 4.975$. The curvature of chiral phase boundary is found to be $\kappa_2 = 0.0184$ in our low energy effective theory. Note that κ_2 here is different from the coefficients in (16), more details about the curvature of phase boundary can be found, e.g., [14,47]. The critical temperature in the chiral limit $T_c^0 = 142.6$ MeV is obtained from fRG calculation in [58]. The scaling variable $z_c = |z_c| e^{i\frac{\pi}{2\beta\delta}}$ with $|z_c| = 1.665$ and $z_0 \in [1,2]$ are suggested in [29]. With the inputs above, one could estimate the convergence radius of Lee-Yang edge singularities via (22). The locations of Lee-Yang edge singularities can also be calculated [33,59]. Moreover, the Roberge-Weiss critical end point is associated with Lee-Yang singularities [23,60], which is located at $\mu_q^{\text{RW}} = i\frac{\pi}{3}T$, i.e., $\hat{\mu}_B^{\text{RW}} = i\pi$ [49,61]. The

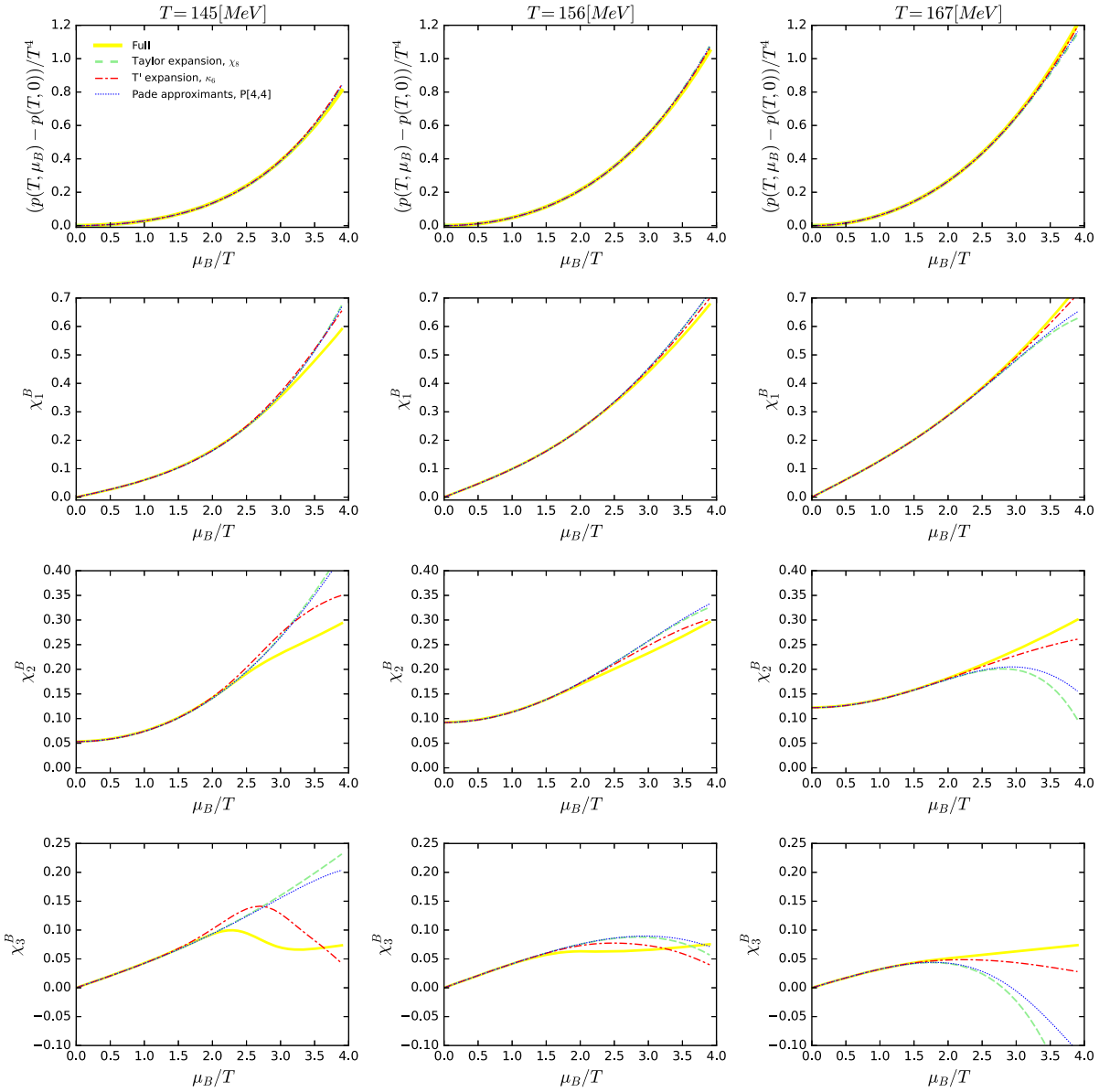

FIG. 4. Comparison between the direct calculations of the pressure and the first three order generalized susceptibilities and those with the Taylor expansion, Padé approximants and the T' expansion, as functions of the baryon chemical potential divided by the temperature μ_B/T at three different values of temperature (different columns).

Roberge-Weiss phase transition temperature is found to be $T^{\mathrm{RW}} = 164$ MeV in our calculations.

In Fig. 6, we show the lines of relative errors 10% for the Taylor expansion, the Padé approximants and the T' expansion of χ_2^B in the plane of T and $\hat{\mu}_B$, and compare them with the Lee-Yang edge singularities estimated above. The left and right plots correspond to the expansion order of $\mathcal{O}(\chi_8^B)$ and $\mathcal{O}(\chi_{10}^B)$, respectively. The Mercer-Roberts estimator $r_{c,6}^{\mathrm{MR}}$ is also shown in the right plot of Fig. 6. The convergence region of the T' expansion becomes small at high temperatures, that has been explained in Sec. III B. The sharp inconsistent region of Padé $P[6,4]$ are caused by the poles of $P[6,4]$ at $T = 146$, 157, 175 MeV, which are also reflected in the Mercer-Roberts estimators $r_{c,6}^{\mathrm{MR}}$. It should be noted that the sharp decrease of estimator convergence radius at several discrete temperatures is nonphysical. We take the ratio estimator as an explanation, i.e., Eq. (13). The χ_n^B for $n \geq 6$ would become zero at several values of temperature, while χ_{n+2}^B at those temperature are nonzero, that will cause the convergence radius of the estimator decreases quickly to zero. This always occurs when one calculates the ratio estimator of high order susceptibilities, which, however, can be got rid of by considering next order

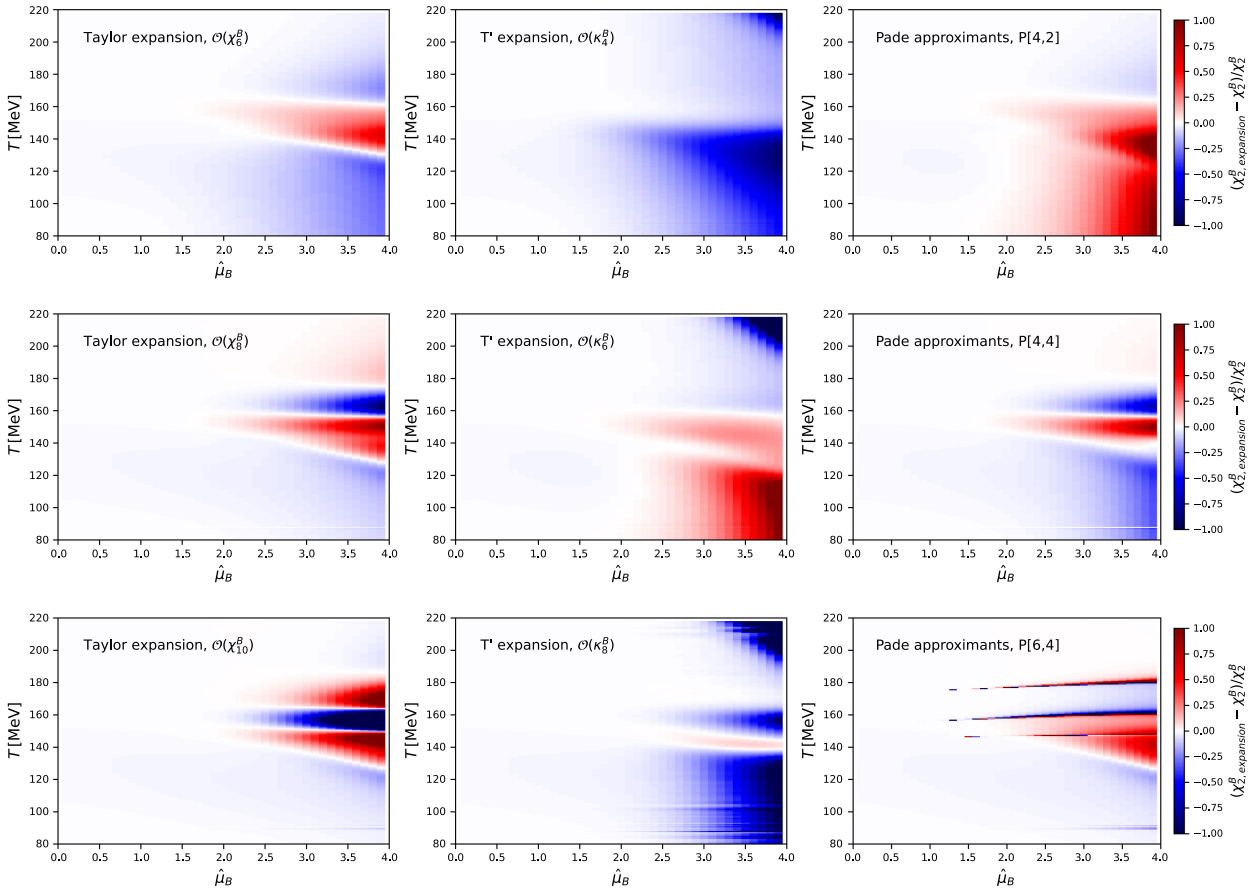

FIG. 5. Relative errors of different expansion schemes for χ_2^B in the plane of T and $\hat{\mu}_B$.

susceptibilities at those temperatures. Ignoring the results of the three values of temperature, one finds that the consistent region of the Padé approximant $P[6,4]$ agrees with that of the Taylor expansion $\mathcal{O}(\chi_{10}^B)$. It is found that all expansion schemes have almost the same convergence region around the critical temperature, and they consist with the Lee-Yang edge singularities. The Roberge-Weiss phase transition singularity is also located within this region. Comparing the left and right plots in Fig. 6, one finds that the convergence region is a bit enlarged by including higher order expansions. Furthermore, we find that the relative error estimates of different expansion schemes are consistent with Lee-Yang edge singularities, while the Mercer-Roberts estimator is not. This might attribute to the fact that our expansion order is still not high enough.

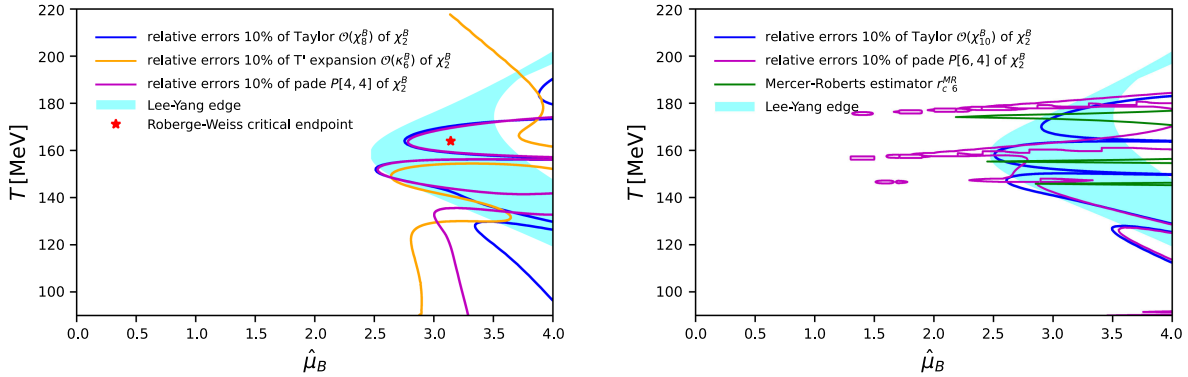

FIG. 6. Lee-Yang edge singularities and relative errors of different expansion schemes up to the order of $\mathcal{O}(\chi_8^B)$ (left panel) and $\mathcal{O}(\chi_{10}^B)$ (right panel) for χ_2^B in the plane of T and $\hat{\mu}_B$. The Mercer-Roberts estimator $r_{c,6}^{\mathrm{MR}}$ is also shown in the right panel.

V. CONCLUSION

In this work, the convergence of different expansion schemes at finite baryon chemical potentials, including the conventional Taylor expansion, the Padé approximants, and the T' expansion proposed recently in lattice QCD simulations, have been investigated in a low energy effective theory within the fRG approach. This is facilitated by the full results of baryon number fluctuations at both real and imaginary chemical potentials, directly calculated in our approach.

We employ two different methods to calculate the expanding coefficients of T' expansion, i.e., fitting the T' at imaginary chemical potentials or using relations between the expanding coefficients of T' expansion and those of Taylor expansion. These two methods provide us with consistent results, which are also comparable to lattice simulations.

The pressure is obtained within the three different expansion schemes all up to the expanding order $\mathcal{O}(\mu_B^8)$, from which we calculate the baryon number fluctuations of first three orders, i.e., χ_1^B, χ_2^B, χ_3^B. The pressure and the fluctuations of first three orders are found to be consistent with the full results within the regions $\mu_B/T \lesssim 3.5, 3.0, 2.0, 1.5$, respectively. The consistent region near the critical temperature is smaller than those at high or low temperature. We also compare the results obtained with the expansion order up to $\mathcal{O}(\mu_B^6)$, $\mathcal{O}(\mu_B^8)$, and $\mathcal{O}(\mu_B^{10})$, which indicates that it could enlarge a bit the consistent region by including higher-order expansions. It is found that the T' expansion or the Padé approximants would hardly improve the convergence of expansion in comparison to the conventional Taylor expansion, within the expansion orders considered in this work. Furthermore, We also estimate the singularities in the complex plane of chemical potential, arising from the Lee-Yang edge singularities and Roberge-Weiss phase transition. The consistent regions of the three different expansions are in agreement with the convergence radius of the Lee-Yang edge singularities.

ACKNOWLEDGMENTS

We thank Mei Huang and Yang-yang Tan for their valuable discussions. This work is supported by the National Natural Science Foundation of China under Grant No. 12175030 and Fundamental Research Funds for the Central Universities No. E3E46301X2. This work is supported by the Alexander von Humboldt foundation.

APPENDIX: EXPRESSIONS OF THE PADÉ APPROXIMANTS AND T' EXPANSION

In this Appendix, we show the expressions of the Padé approximants and T' expansion up to the order of $\mathcal{O}(\chi_{10}^B)$.

1. Padé approximants

By solving Eq. (12), we arrive at

$$P[4,2] = \frac{60\chi_2^B\chi_4^B\hat{\mu}_B^2 + (5(\chi_4^B)^2 - 2\chi_2^B\chi_6^B)\mu_B^4}{120\chi_4^B - 4\chi_6^B\hat{\mu}_B^2}, \tag{A1}$$

$$\begin{aligned} P[4,4] = {} & \big[2520\chi_2^B(-5(\chi_4^B)^2 + 2\chi_2^B\chi_6^B)\hat{\mu}_B^2 - 30(35(\chi_4^B)^3 \\ & - 28\chi_2^B\chi_4^B\chi_6^B + 3(\chi_2^B)^2\chi_8^B)\mu_B^4\big]\big[5040 \\ & \times(-5(\chi_4^B)^2 + 2\chi_2^B\chi_6^B) + 60(14\chi_4^B\chi_6^B \\ & - 3\chi_2^B\chi_8^B)\hat{\mu}_B^2 + (-28(\chi_6^B)^2 + 15\chi_4^B\chi_8^B)\hat{\mu}_B^4\big]^{-1}, \end{aligned} \tag{A2}$$

$$\begin{aligned} P[6,4] = {} & \big[5040\chi_2^B(28\chi_6^{B2} - 15\chi_4^B\chi_8^B)\hat{\mu}_B^2 + 420(2\chi_{10}^B\chi_2^B\chi_4^B + 28\chi_4^B\chi_6^{B2} \\ & - 15\chi_4^{B2}\chi_8^B - 6\chi_2^B\chi_6^B\chi_8^B)\mu_B^4 + (70\chi_{10}^B\chi_4^{B2} - 28\chi_{10}^B\chi_2^B\chi_6^B + 392\chi_6^{B3} \\ & - 420\chi_4^B\chi_6^B\chi_8^B + 45\chi_2^B\chi_8^{B2})\mu_B^6\big]\big[2(5040(28\chi_6^{B2} - 15\chi_4^B\chi_8^B) \\ & + 840(\chi_{10}^B\chi_4^B - 3\chi_6^B\chi_8^B)\mu_B^2 + (-28\chi_{10}^B\chi_6^B + 45\chi_8^{B2})\mu_B^4)\big]^{-1}, \end{aligned} \tag{A3}$$

where the expression of $P[4,4]$ is also shown in [39].

2. T' expansion

Comparing (17) with (15) and (16), one obtains the relations between the two sets of expansion coefficients,

$$\frac{\chi_4^B(T)}{3!} = \frac{\partial\chi_2^B}{\partial T}T\kappa_2^B(T), \tag{A4}$$

$$\frac{\chi_6^B(T)}{5!} = \frac{\partial\chi_2^B}{\partial T}T\kappa_4^B(T) + \frac{1}{2!}\frac{\partial^2\chi_2^B}{(\partial T)^2}T^2(\kappa_2^B(T))^2, \tag{A5}$$

$$\begin{aligned} \frac{\chi_8^B(T)}{7!} = {} & \frac{\partial\chi_2^B}{\partial T}T\kappa_6^B(T) + \frac{1}{2!}\frac{\partial^2\chi_2^B}{(\partial T)^2}T^2(2\kappa_2^B(T)\kappa_4^B(T)) \\ & + \frac{1}{3!}\frac{\partial^3\chi_2^B}{(\partial T)^3}T^3(\kappa_2^B(T))^3, \end{aligned} \tag{A6}$$

$$\frac{\chi_{10}^B(T)}{9!} = \frac{\partial\chi_2^B}{\partial T}T\kappa_8^B(T) + \frac{1}{2!}\frac{\partial^2\chi_2^B}{(\partial T)^2}T^2(2\kappa_2^B(T)\kappa_6^B(T) + (\kappa_4^B(T))^2) + \frac{1}{2}\frac{\partial^3\chi_2^B}{(\partial T)^3}T^3(\kappa_2^B(T))^2\kappa_4^B(T) + \frac{1}{4!}\frac{\partial^4\chi_2^B}{(\partial T)^4}T^4(\kappa_2^B(T))^4. \tag{A7}$$

$$\kappa_2^B = \frac{\chi_4^B}{6T\chi_2^{B\prime}}, \tag{A8}$$

$$\kappa_4^B = \frac{3(\chi_2^{B\prime})^2\chi_6^B - 5\chi_2^{B\prime\prime}(\chi_4^B)^2}{360T(\chi_2^{B\prime})^3}, \tag{A9}$$

$$\kappa_6^B = \left[105(\chi_2^{B\prime\prime})^2(\chi_4^B)^3 - 63\chi_2^{B\prime\prime}(\chi_2^{B\prime})^2\chi_4^B\chi_6^B - 35\chi_2^{B\prime\prime\prime} \times \chi_2^{B\prime}(\chi_4^B)^3 + 9(\chi_2^{B\prime})^4\chi_8^B\right]\left[45360(\chi_2^{B\prime})^5T\right]^{-1}, \tag{A10}$$

Then, the coefficients in turn can be solved order by order,

$$\kappa_8^B = -\left[2625(\chi_2^{B\prime\prime})^3(\chi_4^B)^4 + 35(\chi_2^{B\prime})^2(5\chi_2^{B(4)}\chi_4^{B4} - 54(\chi_2^{B\prime\prime})^2(\chi_4^B)^2\chi_6^B) - 1750\chi_2^{B\prime\prime}\chi_2^{B(3)}\chi_2^{B\prime}(\chi_4^B)^4 + 9\chi_2^{B\prime\prime}(\chi_2^{B\prime})^4(20\chi_4^B\chi_8^B + 21(\chi_6^B)^2) + 630\chi_2^{B(3)}(\chi_2^{B\prime})^3(\chi_4^B)^2\chi_6^B - 15(\chi_2^{B\prime})^6\chi_{10}^B\right]\left[5443200(\chi_2^{B\prime})^7T\right]^{-1}. \tag{A11}$$

Here, the prime, e.g., $\chi_2^{B\prime}$, denotes the derivative with respect to the temperature.

[1] J. Adam *et al.* (STAR Collaboration), Nonmonotonic energy dependence of net-proton number fluctuations, Phys. Rev. Lett. **126**, 092301 (2021).

[2] M. Abdallah *et al.* (STAR Collaboration), Cumulants and correlation functions of net-proton, proton, and antiproton multiplicity distributions in Au + Au collisions at energies available at the BNL relativistic heavy ion collider, Phys. Rev. C **104**, 024902 (2021).

[3] M. Abdallah *et al.* (STAR Collaboration), Measurement of the sixth-order cumulant of net-proton multiplicity distributions in Au + Au collisions at $\sqrt{s_{NN}} = 27$, 54.4, and 200 GeV at RHIC, Phys. Rev. Lett. **127**, 262301 (2021).

[4] M. S. Abdallah *et al.* (STAR Collaboration), Measurements of proton high order cumulants in $\sqrt{s_{\mathrm{NN}}} = 3$ GeV Au + Au collisions and implications for the QCD critical point, Phys. Rev. Lett. **128**, 202303 (2022).

[5] A. Pandav (STAR Collaboration), Measurement of cumulants of conserved charge multiplicity distributions in Au + Au collisions from the STAR experiment, Nucl. Phys. **A1005**, 121936 (2021).

[6] A. Bazavov *et al.*, Equation of state and QCD transition at finite temperature, Phys. Rev. D **80**, 014504 (2009).

[7] A. Bazavov *et al.* (HotQCD Collaboration), Equation of state in (2 + 1)-flavor QCD, Phys. Rev. D **90**, 094503 (2014).

[8] S. Borsanyi, Z. Fodor, C. Hoelbling, S. D. Katz, S. Krieg, and K. K. Szabo, Full result for the QCD equation of state with 2 + 1 flavors, Phys. Lett. B **730**, 99 (2014).

[9] A. Bazavov *et al.* (HotQCD Collaboration), Skewness and kurtosis of net baryon-number distributions at small values of the baryon chemical potential, Phys. Rev. D **96**, 074510 (2017).

[10] S. Borsanyi, Z. Fodor, J. N. Guenther, S. K. Katz, K. K. Szabo, A. Pasztor, I. Portillo, and C. Ratti, Higher order fluctuations and correlations of conserved charges from lattice QCD, J. High Energy Phys. 10 (2018) 205.

[11] A. Bazavov *et al.*, Skewness, kurtosis, and the fifth and sixth order cumulants of net baryon-number distributions from lattice QCD confront high-statistics STAR data, Phys. Rev. D **101**, 074502 (2020).

[12] S. Borsányi, Z. Fodor, J. N. Guenther, S. D. Katz, P. Parotto, A. Pásztor, D. Pesznyák, K. K. Szabó, and C. H. Wong, Continuum extrapolated high order baryon fluctuations, arXiv:2312.07528.

[13] D. Bollweg, J. Goswami, O. Kaczmarek, F. Karsch, S. Mukherjee, P. Petreczky, C. Schmidt, and P. Scior (HotQCD Collaboration), Second order cumulants of conserved charge fluctuations revisited: Vanishing chemical potentials, Phys. Rev. D **104**, 074512 (2021).

[14] W.-j. Fu, J. M. Pawlowski, and F. Rennecke, QCD phase structure at finite temperature and density, Phys. Rev. D **101**, 054032 (2020).

[15] J. Braun, W.-j. Fu, J. M. Pawlowski, F. Rennecke, D. Rosenblüh, and S. Yin, Chiral susceptibility in (2 + 1)-flavor QCD, Phys. Rev. D **102**, 056010 (2020).

[16] M. Mitter, J. M. Pawlowski, and N. Strodthoff, Chiral symmetry breaking in continuum QCD, Phys. Rev. D **91**, 054035 (2015).

[17] A. K. Cyrol, M. Mitter, J. M. Pawlowski, and N. Strodthoff, Nonperturbative quark, gluon, and meson correlators of unquenched QCD, Phys. Rev. D **97**, 054006 (2018).

[18] J. Braun, L. Fister, J. M. Pawlowski, and F. Rennecke, From quarks and gluons to hadrons: Chiral symmetry breaking in dynamical QCD, Phys. Rev. D **94**, 034016 (2016).

[19] F. Gao and J. M. Pawlowski, Chiral phase structure and critical end point in QCD, Phys. Lett. B **820**, 136584 (2021).
[20] J. Bernhardt, C. S. Fischer, P. Isserstedt, and B.-J. Schaefer, Critical endpoint of QCD in a finite volume, Phys. Rev. D **104**, 074035 (2021).
[21] P. Isserstedt, M. Buballa, C. S. Fischer, and P. J. Gunkel, Baryon number fluctuations in the QCD phase diagram from Dyson-Schwinger equations, Phys. Rev. D **100**, 074011 (2019).
[22] Y. Lu, F. Gao, Y.-X. Liu, and J. M. Pawlowski, QCD equation of state and thermodynamic observables from computationally minimal Dyson-Schwinger Equations, arXiv:2310.18383.
[23] J. N. Guenther, An overview of the QCD phase diagram at finite T and μ, *Proc. Sci.*, LATTICE2021 (2022) 013 [arXiv:2201.02072].
[24] J. N. Guenther, Overview of the QCD phase diagram: Recent progress from the lattice, Eur. Phys. J. A **57**, 136 (2021).
[25] N. Dupuis, L. Canet, A. Eichhorn, W. Metzner, J. M. Pawlowski, M. Tissier, and N. Wschebor, The nonperturbative functional renormalization group and its applications, Phys. Rep. **910**, 1 (2021).
[26] F. Rennecke, Review of critical point searches and beam-energy studies, MDPI Proc. **10**, 8 (2019).
[27] W.-j. Fu, QCD at finite temperature and density within the fRG approach: An overview, Commun. Theor. Phys. **74**, 097304 (2022).
[28] A. Bazavov *et al.*, The QCD equation of state to $\mathcal{O}(\mu_B^6)$ from lattice QCD, Phys. Rev. D **95**, 054504 (2017).
[29] S. Mukherjee and V. Skokov, Universality driven analytic structure of the QCD crossover: Radius of convergence in the baryon chemical potential, Phys. Rev. D **103**, L071501 (2021).
[30] S. Borsanyi, Z. Fodor, S. D. Katz, S. Krieg, C. Ratti, and K. K. Szabo, Freeze-out parameters: Lattice meets experiment, Phys. Rev. Lett. **111**, 062005 (2013).
[31] G. Basar, G. V. Dunne, and Z. Yin, Uniformizing Lee-Yang singularities, Phys. Rev. D **105**, 105002 (2022).
[32] A. Connelly, G. Johnson, F. Rennecke, and V. Skokov, Universal location of the Yang-Lee edge singularity in $O(N)$ theories, Phys. Rev. Lett. **125**, 191602 (2020).
[33] S. Mukherjee, F. Rennecke, and V. V. Skokov, Analytical structure of the equation of state at finite density: Resummation versus expansion in a low energy model, Phys. Rev. D **105**, 014026 (2022).
[34] F. Karsch, C. Schmidt, and S. Singh, Lee-Yang and Langer edge singularities from analytic continuation of scaling functions, Phys. Rev. D **109**, 014508 (2024).
[35] V. Vovchenko, J. Steinheimer, O. Philipsen, and H. Stoecker, Cluster expansion model for QCD baryon number fluctuations: No phase transition at $\mu_B/T < \pi$, Phys. Rev. D **97**, 114030 (2018).
[36] F. Karsch, B.-J. Schaefer, M. Wagner, and J. Wambach, Towards finite density QCD with Taylor expansions, Phys. Lett. B **698**, 256 (2011).
[37] S. Datta, R. V. Gavai, and S. Gupta, Quark number susceptibilities and equation of state at finite chemical potential in staggered QCD with $\mathrm{Nt} = 8$, Phys. Rev. D **95**, 054512 (2017).
[38] A. Pásztor, Z. Szép, and G. Markó, Apparent convergence of Padé approximants for the crossover line in finite density QCD, Phys. Rev. D **103**, 034511 (2021).
[39] D. Bollweg, J. Goswami, O. Kaczmarek, F. Karsch, S. Mukherjee, P. Petreczky, C. Schmidt, and P. Scior (HotQCD Collaboration), Taylor expansions and Padé approximants for cumulants of conserved charge fluctuations at nonvanishing chemical potentials, Phys. Rev. D **105**, 074511 (2022).
[40] S. Mondal, S. Mukherjee, and P. Hegde, Lattice QCD equation of state for nonvanishing chemical potential by resumming Taylor expansions, Phys. Rev. Lett. **128**, 022001 (2022).
[41] S. Borsanyi, Z. Fodor, M. Giordano, S. D. Katz, D. Nogradi, A. Pasztor, and C. H. Wong, Lattice simulations of the QCD chiral transition at real baryon density, Phys. Rev. D **105**, L051506 (2022).
[42] A. Pasztor, S. Borsanyi, Z. Fodor, K. Kapas, S. D. Katz, M. Giordano, D. Nogradi, and C. H. Wong, New approach to lattice QCD at finite density: Reweighting without an overlap problem, *Proc. Sci.*, LATTICE2021 (2022) 128 [arXiv:2112.02134].
[43] S. Borsanyi, Z. Fodor, M. Giordano, J. N. Guenther, S. D. Katz, A. Pasztor, and C. H. Wong, Equation of state of a hot-and-dense quark gluon plasma: Lattice simulations at real μB vs extrapolations, Phys. Rev. D **107**, L091503 (2023).
[44] S. Borsányi, Z. Fodor, J. N. Guenther, R. Kara, S. D. Katz, P. Parotto, A. Pásztor, C. Ratti, and K. K. Szabó, Lattice QCD equation of state at finite chemical potential from an alternative expansion scheme, Phys. Rev. Lett. **126**, 232001 (2021).
[45] S. Borsanyi, J. N. Guenther, R. Kara, Z. Fodor, P. Parotto, A. Pasztor, C. Ratti, and K. K. Szabo, Resummed lattice QCD equation of state at finite baryon density: Strangeness neutrality and beyond, Phys. Rev. D **105**, 114504 (2022).
[46] W.-j. Fu and J. M. Pawlowski, Relevance of matter and glue dynamics for baryon number fluctuations, Phys. Rev. D **92**, 116006 (2015).
[47] W.-j. Fu, X. Luo, J. M. Pawlowski, F. Rennecke, R. Wen, and S. Yin, Hyper-order baryon number fluctuations at finite temperature and density, Phys. Rev. D **104**, 094047 (2021).
[48] W.-j. Fu, X. Luo, J. M. Pawlowski, F. Rennecke, and S. Yin, Ripples of the QCD critical point, arXiv:2308.15508.
[49] K.-x. Sun, R. Wen, and W.-j. Fu, Baryon number probability distribution at finite temperature, Phys. Rev. D **98**, 074028 (2018).
[50] W.-j. Fu, J. M. Pawlowski, F. Rennecke, and B.-J. Schaefer, Baryon number fluctuations at finite temperature and density, Phys. Rev. D **94**, 116020 (2016).
[51] S. Yin, R. Wen, and W.-j. Fu, Mesonic dynamics and the QCD phase transition, Phys. Rev. D **100**, 094029 (2019).
[52] J. M. Pawlowski and F. Rennecke, Higher order quark-mesonic scattering processes and the phase structure of QCD, Phys. Rev. D **90**, 076002 (2014).
[53] R. Wen, C. Huang, and W.-J. Fu, Baryon number fluctuations in the $2+1$ flavor low energy effective model, Phys. Rev. D **99**, 094019 (2019).
[54] P. J. Gunkel and C. S. Fischer, Locating the critical endpoint of QCD: Mesonic backcoupling effects, Phys. Rev. D **104**, 054022 (2021).

[55] B.-J. Schaefer and J. Wambach, The phase diagram of the quark meson model, Nucl. Phys. **A757**, 479 (2005).
[56] Y.-r. Chen, R. Wen, and W.-j. Fu, Critical behaviors of the $O(4)$ and $Z(2)$ symmetries in the QCD phase diagram, Phys. Rev. D **104**, 054009 (2021).
[57] M. Wagner, A. Walther, and B.-J. Schaefer, On the efficient computation of high-order derivatives for implicitly defined functions, Comput. Phys. Commun. **181**, 756 (2010).
[58] J. Braun *et al.*, Soft modes in hot QCD matter, arXiv:2310.19853.
[59] Z.-y. Wan, Y. Lu, F. Gao, and Y.-x. Liu, Lee-Yang edge singularities in QCD via the Dyson-Schwinger equations, arXiv:2401.04957.
[60] D. A. Clarke, K. Zambello, P. Dimopoulos, F. Di Renzo, J. Goswami, G. Nicotra, C. Schmidt, and S. Singh, Determination of Lee-Yang edge singularities in QCD by rational approximations, *Proc. Sci.*, LATTICE2022 (2023) 164 [arXiv:2301.03952].
[61] J. Braun, L. M. Haas, F. Marhauser, and J. M. Pawlowski, Phase structure of two-flavor QCD at finite chemical potential, Phys. Rev. Lett. **106**, 022002 (2011).